

Asymmetric electron localization in the single-photon dissociative ionization of H₂Jun-Ping Wang¹ and Feng He^{2,3,*}¹*College of Physics, Liaoning University, Shenyang 110036, China*²*Key Laboratory for Laser Plasmas (Ministry of Education) and School of Physics and Astronomy, Shanghai Jiao Tong University, Shanghai 200240, China*³*Collaborative innovation center of IFSA (CICIFSA), Shanghai Jiao Tong University, Shanghai 200240, China*

(Received 2 June 2021; accepted 21 September 2021; published 1 October 2021)

By numerically solving the non-Born-Oppenheimer time-dependent Schrödinger equation of H₂ in which the dynamics is confined along the laser polarization direction, we study the electron localization in the single-photon dissociative ionization of H₂. The single ionization of H₂ produces a free electron and H₂⁺, in whose later propagation the Coulomb field of the freed electron may excite H₂⁺ from the 1σ_g state to 2pσ_u state. The mixture of these two states with opposite parities results in the asymmetric electron localization on the two nuclei after the dissociation of H₂⁺. The simulation result shows that the bound electron prefers being located on the nucleus, which propagates oppositely to the freed electron. The asymmetry parameter is larger if the freed electron has lower energy. The simulation results agree with experimental measurements in the full energy range. This study indicates that the correlation between H₂⁺ and the freed electron can be important and offers a perspective of controlling electron localization in chemical reactions.

DOI: [10.1103/PhysRevA.104.043101](https://doi.org/10.1103/PhysRevA.104.043101)**I. INTRODUCTION**

The correlation between electrons and nuclei in molecules has brought many fascinating phenomena in the interaction between molecules and strong laser fields. As the simplest neutral molecule in nature, H₂ has been extensively studied, and many ultrafast dynamics in intense laser fields have been demonstrated and explained (see Refs. [1–3] and references therein). For example, the vibrationally resolved photoelectron spectra of H₂ can be used to reconstruct the associated subfemtosecond autoionization dynamics by using the ultrafast nuclear dynamics as an internal clock [4]. Using an advanced attosecond pump-probe spectroscopic technology, it is shown that the coupling between electronic and nuclear motion in the H₂ molecule is reflected in the phase of the entangled electron-nuclear wave packet, which depends on the energy distribution between electrons and nuclei [5]. Through the use of coincidence measurement technology, it is confirmed that the electron-nuclear correlated multiphoton resonant excitation is the general mechanism in producing Rydberg fragments of a breaking molecule [6]. By comparing the dynamic processes between H₂ and D₂, one can obtain the influence of nuclear masses on the ultrafast process, for example, different tunneling ionization rate [7,8] and different high harmonic generation [9–11].

For H₂, electrons experience spatially symmetric Coulomb potential, and thus the electron wave function has either even or odd parities. Electrons distribute symmetrically on the two atomic nuclei. By introducing an external laser field, such

symmetry may be broken. Many schemes have been implemented to break the symmetric localization in the dissociative ionization of H₂. Kling *et al.* [12] used a carrier-envelope phase-locked few-cycle laser pulse to control the electron localization, which confirmed the theoretical prediction [13]. Ray *et al.* [14] used two-color pulses to control the interference between the two dissociative channels. To enhance the degree of asymmetry, He *et al.* [15] used the attosecond pulse to initiate molecular dissociation, and a time-delayed few-cycle infrared laser pulse to steer the electron movement. Later, Sansone *et al.* [16] implemented such a pump-probe strategy and observed delay-dependent electron localization in an experiment. Instead of using an isolated pulse, He *et al.* [17] also suggested using an attosecond pulse train plus an infrared pulse to control the electron localization, which had been confirmed in the experiment [18]. Some other strategies of controlling electron localization are also realized, such as single circularly polarized multicycle laser pulse [19], phase-controlled elliptically polarized or orthogonally polarized two-color laser pulses [20,21]. The mechanism governing asymmetric electron localization can be understood in two consistent ways. In one way, the electron hopping between two nuclei is prohibited by the increasing Coulomb barrier between two nuclei during the molecular dissociation, and thus the electron simply locates at the position before the barrier blocks the electron movement. In another way, the laser mixes the 1σ_g and 2pσ_u states, which have odd and even parities, and it is the superposition that breaks the symmetric electron distribution.

At present, the theoretical study of the electron localization in dissociative ionization of H₂ is approximated by a two-step model [14,22–24]. In the first step, the H₂ undergoes single

*fhe@sjtu.edu.cn

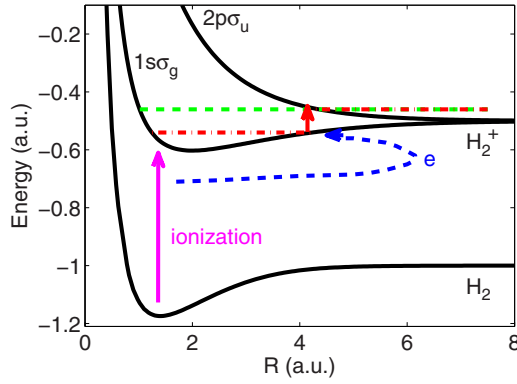


FIG. 1. The related potential curves for the ultrafast reaction of H_2 in strong laser fields and the sketch of electron localization induced by the Coulomb field of the ionized electron. The green dashed line indicates that H_2^+ is in the vibration continuum state of $1s\sigma_g$, and the red dash-dotted line indicates that H_2^+ is initially in the vibration bound state of $1s\sigma_g$ and excited to the $2p\sigma_u$ state by the Coulomb field of the ionized electron.

ionization to generate a vibrationally excited H_2^+ wave packet, which is described by the Franck-Condon approximation; in the second step, the H_2^+ wave packet evolves along the $1s\sigma_g$ potential energy curve, meanwhile, the remaining laser field dissociates H_2^+ . In the second step, the correlation between H_2^+ and the electron released in the first step is usually neglected. Recently, Serov and Kheifets [25] predicted that after single ionization of H_2 , the Coulomb interaction between the freed electron and the vibrating H_2^+ may pump H_2^+ from the $1s\sigma_g$ state to the $2p\sigma_u$ state. Such a mixture of the two states results in the electron asymmetric distribution on the two nuclei during H_2^+ dissociation. Subsequently, Waitz *et al.* [26] and Heck *et al.* [27] experimentally observed this asymmetric distribution. However, the theoretical model of Serov and Kheifets may give satisfied agreement in some energy ranges between the experiment and theory, but it does not work if the freed electron has very low energy. To fully recover the experiment measurement, the best way is to perform *ab initio* calculations. To the best of our knowledge, there are still no quantum mechanical calculations beyond the Born-Oppenheimer approximation for the retroaction of the Coulomb field of the photoelectron on its parent ion.

In this paper, we study the effect of the ejected electron in the single ionization of H_2 on the localization of the bound electron in H_2^+ by numerically solving the time-dependent Schrödinger equation (TDSE). The XUV pulse has the photon energy 21.1 eV and pulse duration 12 fs. The theoretical scheme is shown in Fig. 1. The H_2 molecule is ionized by the XUV pulse, generating a free electron and H_2^+ . Since the XUV photon energy is slightly larger than 18.1 eV, the ionization potential of H_2 , only the $1s\sigma_g$ state of H_2^+ can be reached. Once the nuclear wave packet moves to a region where the $2p\sigma_u$ potential energy curve is very close to the $1s\sigma_g$ potential energy curve, the Coulomb field generated by the ejected electron excites H_2^+ from the $1s\sigma_g$ state to the $2p\sigma_u$ state (as shown by the red arrow in Fig. 1). Finally, H_2^+ dissociates along either the $1s\sigma_g$ state or the $2p\sigma_u$ state, resulting in the electron asymmetric localization on the two nuclei. The rest

of the paper is organized as follows. In Sec. II, we introduce the details of our simulation model. In Sec. III, we show the numerical results. The paper ends with a short summary in Sec. IV.

II. NUMERICAL MODELS

The dissociative ionization of H_2 in strong laser fields is governed by the TDSE (atomic units, $e = m = \hbar = 1$, are used unless indicated otherwise)

$$i \frac{\partial}{\partial t} \Psi(R, x_1, x_2; t) = [T + V(R, x_1, x_2)] \Psi(R, x_1, x_2; t), \quad (1)$$

with the kinetic energy operator

$$T = \frac{p_R^2}{2\mu} + \frac{[p_1 + A(t)]^2}{2} + \frac{[p_2 + A(t)]^2}{2} \quad (2)$$

and the potential

$$V(R, x_1, x_2) = \frac{1}{R} + \frac{1}{\sqrt{(x_1 - x_2)^2 + \alpha(R)}} - \sum_{s=\pm 1} \sum_{i=1,2} \frac{1}{\sqrt{(x_i + sR/2)^2 + \frac{\beta(R)^2}{25} + \frac{1}{\beta(R)} - \frac{\beta(R)}{5}}}. \quad (3)$$

In Eq. (2), μ is the reduced nuclear mass, $A(t)$ is the laser vector potential, and $A(t) = -\int_{-\infty}^t E(t') dt'$ with $E(t)$ being the electric field. $\alpha(R)$ and $\beta(R)$ represent soft-core parameters, and their values are shown in Fig. 2 of Ref. [28]. With the proper R -dependent soft-core parameters, the calculated Born-Oppenheimer energy curves shown in Fig. 1 almost quantitatively agree with the real ones and thus the simplified one-dimensional model is good enough for analyzing the dynamics [29,30]. By the way, this similar numerical model has been used to study the double ionization of H_2 [31,32] and high-harmonic-order generation [33], above-threshold dissociation and ionization [34].

In simulations, the spatial grids are $\Delta x_1 = \Delta x_2 = 0.3$ a.u. and $\Delta R = 0.04$ a.u., and the time step is $\Delta t = 0.1$ a.u.. Simulation convergence has been tested by using smaller time-spatial grids. The simulation box along x_1 - x_2 - R are sampled by the grids $11\ 100 \times 170 \times 1100$. To suppress the unphysical reflection, a mask function $\cos^{1/6}$ is used in the boundaries of the simulation box. In calculations, the ionization wave packet of the electron represented by x_2 is absorbed by the numerical boundaries, but x_1 is large enough to hold all ionized wave packets of the electron represented by x_1 . Please note that the different sizes for x_1 and x_2 break the two-electron permutation symmetry. Nevertheless, such a treatment does not blur the simulated asymmetry parameter because of the following reasons. In this study, we only care about the dissociative ionization, which means one electron is very close to the nuclei and the other electron is far away from the nuclei. The two-electron wave functions nearly have no spatial overlap, therefore the identical particle effects (such as exchange force) does not appear. The only care here is that half of the dissociative ionization events are not contained since the ionization of x_2 is absorbed by the boundaries. The initial state was obtained by propagating the

field-free Schrödinger equation in imaginary time [35]. In both the real-time and imaginary-time propagation, we used the Crank-Nicolson method of second-order implicit difference to propagate the wave packet [36]. The linearly polarized laser field is written as

$$E(t) = E_0 \sin(\omega t) \sin^2\left(\frac{\pi t}{\tau}\right), \quad (4)$$

where E_0 , ω , and τ are the amplitude, frequency, and pulse width of the XUV pulse, respectively. The amplitude relates to the intensity by $E_0 = \sqrt{I/(3.51 \times 10^{16} \text{ W/cm}^2)}$ with I being the laser intensity. In simulations, we keep propagating the wave function until $t_{\text{end}} = 3500$ a.u., at which time the energetic freed electron, hydrogen atom, and the proton are far away from each other and the Coulomb potential is negligible. To obtain the wave function in momentum representation, at the end of the calculations, we Fourier transform the wave function. However, for photoelectrons with very low energies, the Fourier transformation cannot give an accurate electron energy distribution, and other methods such as a window operator [37] are needed. In the present work, where the photoelectron energy is higher than 0.5 eV, the results are not affected by such numerical inaccuracy.

III. SIMULATION RESULTS

Exposing H_2 into XUV fields, two typical pathways may occur. In the first case, one electron may carry all the excess energy and H_2^+ in the $1s\sigma_g$ state is formed. Hence, H_2^+ has a large probability to remain bound, however, H_2^+ with the nuclear energy higher than the dissociation limit will finally dissociate into a proton and a hydrogen atom. In the second case, if the photon energy is big enough, the photon energy may be shared by the two electrons, knocking out one electron and exciting the other one by forming H_2^+ in the $2p\sigma_u$ state. The above two channels can be formulated as $\text{H}_2 + \gamma \rightarrow e^- + \text{H}_2^+(1s\sigma_g)$, and $\text{H}_2 + \gamma \rightarrow e^- + \text{H}_2^+(2p\sigma_u) \rightarrow e^- + \text{H} + \text{p}$, respectively. In our simulations, the photon energy is fixed at $E_\gamma = 21.1$ eV, which is not big enough to initiate the second channel. The laser pulse width is $\tau = 60T$, where T is the optical period of the laser field, and the laser intensity is $I = 10^{14} \text{ W/cm}^2$. The theoretical scheme is shown in Fig. 1. In the single-photon dissociative ionization of H_2 , it is expected and experimentally verified to have symmetric electron localization since only one dissociation channel participates the dissociation process [38–42]. However, recent theoretical and experimental studies [25–27] reexamined that asymmetric electron localization on two nuclei may still happen due to the Coulomb coupling between the freed electron and the dissociating H_2^+ .

Here, we numerically solve the TDSE to study the physical mechanism of asymmetric electron localization. Figure 2 shows the snapshots of wave-function distributions in the x_1 - R space, i.e., $W(x_1, R; t) = \int |\Psi(x_1, x_2, R; t)|^2 dx_2$ at [Fig. 2(a)] $t = 0$, [Fig. 2(b)] $t = 200$, [Fig. 2(c)] $t = 400$, and [Fig. 2(d)] $t = 700$ a.u. What is shown in Fig. 2(a) is actually the ground-state distribution. In Fig. 2(b), one can see that some wave packets start to propagate out, whereas some parts remain in the ground state. With the time evolution, as shown in Fig. 2(c), the photoelectron may escape with different ve-

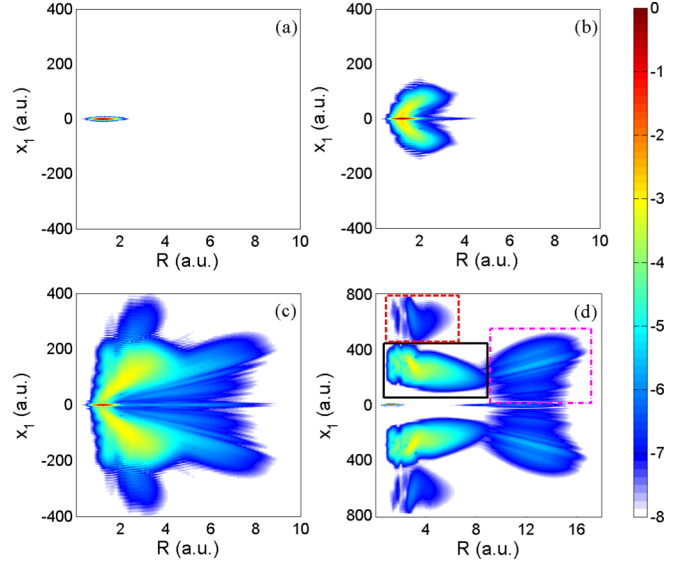


FIG. 2. The snapshots of wave-function distributions in $x_1 - R$ space at (a) $t = 0$, (b) $t = 200$, (c) $t = 400$, and (d) $t = 700$ a.u. in the logarithm scale. The wave function marked with a red dashed rectangle corresponds to forming a freed electron and bound H_2^+ . The wave function marked with a pink dash-dotted rectangle corresponds to the second pathway of producing H_2^+ in the $2p\sigma_u$ state. The wave function in the black solid rectangle indicates H_2^+ in the $1s\sigma_g$ state after single ionization of H_2 , but part of the wave function with relatively high nuclear kinetic energy will dissociate. The laser intensity is $I = 10^{14} \text{ W/cm}^2$.

locities since the photo energy is shared between the freed electron and the nuclei vibration with different manners. In Fig. 2(d), the wave functions already clearly distribute in different areas. The part marked by a red dashed rectangle corresponds to forming a freed electron and bound H_2^+ . The part marked by a pink dash-dotted rectangle corresponds to the second pathway of producing H_2^+ in the $2p\sigma_u$ state. The wave function in the black solid rectangle indicates H_2^+ in the $1s\sigma_g$ state after single ionization of H_2 , but part of the wave function with relative high nuclear kinetic energy will dissociate.

Figure 3 shows the electron-nuclear joint energy spectrum (JES) corresponding to the wave function in the black solid rectangle in Fig. 2(d). The diagonal structure in Fig. 3 shows that electrons and nuclei share the photon energy, i.e., $E_N + E_e = E_\gamma - (I_p + U_p)$, where E_e represents the electron energy, E_N is the sum of the kinetic energy of p and H , I_p represents the ionization potential of the H_2 molecule, and U_p is the ponderomotive energy. It can be seen from Fig. 3 that the smaller the E_N , the greater the probability of dissociative ionization of H_2 . This result is consistent with the experimental measurements in Fig. 1(c) of Ref. [26] and Fig. 2 of Ref. [27].

To quantitatively compare with experimental and theoretical results, we define an asymmetric parameter

$$\delta(E_N, E_e) = \frac{N_l(E_N, E_e) - N_r(E_N, E_e)}{N_l(E_N, E_e) + N_r(E_N, E_e)}, \quad (5)$$

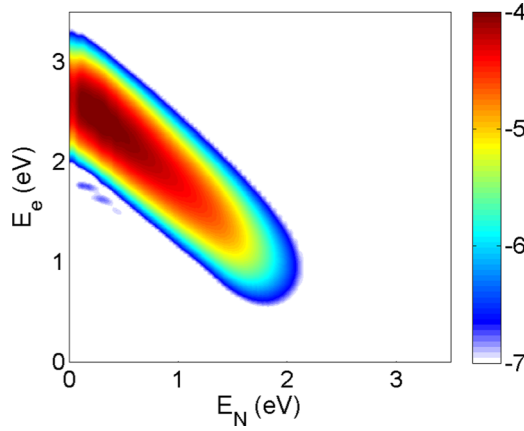


FIG. 3. The electron-nuclear JES. The laser parameters are the same as those used in Fig. 2.

where $N_l(E_N, E_e) = \int_{-x_{2\max}}^0 \frac{|\mu|\tilde{\Psi}(p_1, x_2, p_R; t_{\text{end}})|^2}{|p_1 p_R|} dx_2$, and $N_r(E_N, E_e) = \int_0^{x_{2\max}} \frac{|\mu|\tilde{\Psi}(p_1, x_2, p_R; t_{\text{end}})|^2}{|p_1 p_R|} dx_2$ with $E_N = p_R^2/2\mu$ and $E_e = p_1^2/2$ and $p_1 > 0$, and $\tilde{\Psi}(p_1, x_2, p_R; t_{\text{end}})$ is the dissociative ionized wave packet in the representation p_1 - x_2 - p_R .

Since $p_1 > 0$, N_l and N_r means the probabilities that the freed electron propagates along the positive x axis, and the bound electron locates in the left or right nucleus if H_2 is aligned along the horizontal x axis. $\delta > 0$ means that the ionized electrons and the bound electron are located in the opposite half sphere in the experiments. The asymmetry parameters here are the same as Eq. (3) in Ref. [26] and Eq. (13) in Ref. [25], so that we can make a quantitative comparison with existing experimental and theoretical results. Figure 4 shows the asymmetry parameter δ as a function of the nuclear energy E_N . Among them, the blue solid line is the result of the quantum calculation in this paper, and the red dashed line is the prediction given by Serov and Kheifets [25]. The

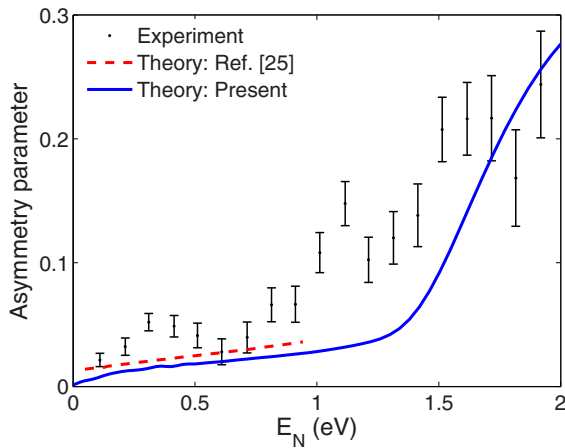


FIG. 4. The asymmetry parameter δ as a function of the nuclear energy E_N . The blue solid line is the result of quantum calculation in this paper. The red dashed line is taken from Ref. [25]. The black points with error bars are taken from Ref. [26]. The photon energy is 21.1 eV.

black points with error bars are the experimental results [26]. One can see that the TDSE simulation results are very close to the theoretical results of treating electrons as classic particles. In the theoretical model of Serov and Kheifets [25], the ejected electron must be far away from the H_2^+ at the time of transition, so that the electron may have a steady velocity v_e and a steady energy E_e with $v_e = \sqrt{2E_e}$. When the ejected electron energy E_e is very small and comparable to the excitation energy of the H_2^+ , the approximate condition will be crude since the energy of the ejected electron E_e will change noticeably after the excitation of the bound electron. Therefore, the validity range of the classical theory is restricted to $E_e \gg E_N$. The comparison between the experimental results and theoretical predictions in [26] can only take a part that satisfies the conditions approximately, i.e., $E_e > \frac{2}{3}E_N$. Our TDSE calculation is not restricted by any conditions, and this calculation makes up for the missing part of the theoretical prediction in Ref. [25]. Compared with the experimental results, our simulation results are in good agreement with the experimental results in all energy ranges.

It can be seen from Fig. 4 that as the E_N increases, the asymmetry parameter becomes larger. Due to the conservation of electron energy and nuclear energy, that is, $E_N + E_e = E_\gamma - (I_p + U_p)$ with U_p the ponderomotive energy and I_p the ionization potential, the smaller the electron energy, the larger the asymmetry parameter. This scenario can be explained by the mechanism that produces asymmetry. After the single-photon ionization of H_2 , H_2^+ experiences the Coulomb field created by the freed electron. Since the strength of the Coulomb field is inversely proportional to the square distance of the free electron from H_2^+ , a faster free electron has less interaction with H_2^+ . The H_2^+ wave packet initially evolves along the $1s\sigma_g$ potential curve. When the nuclear wave packet moves to a region where the $2p\sigma_u$ potential energy curve is very close to the $1s\sigma_g$ potential energy curve, the Coulomb field generated by the free electron excites the part of the nuclear wave packet from the $1s\sigma_g$ state to the $2p\sigma_u$ state. Finally, the dissociated nuclear wave packet is in the superimposed states with even and odd parities, resulting in the asymmetric electron localization on two nuclei in the dissociated H_2^+ . The probability of being excited to the $2p\sigma_u$ state depends on the Coulomb field, and thus depends on the freed electron energy. To further verify the above explanation and exclude the laser-induced coupling between $1s\sigma_g$ and $2p\sigma_u$ states, we artificially neglect the interaction between the laser field and the electron represented by x_2 in the calculation, that is, in Eq. (2), forcing $A(t) = 0$ in the second term, and find that this asymmetric parameter remains the same.

Now, we turn to study the isotope effect on the asymmetric localization. We study the dissociative ionization of D_2 and T_2 in the same laser field. Compared to H_2 , due to the slower nuclear motion in D_2 , the time it takes for the D_2^+ nuclear wave packet to reach critical internuclear distances for transition is longer, so the distance of ionized electrons from D_2^+ is also far away. Thus D_2^+ experiences a weaker Coulomb field, and the corresponding asymmetric parameter is smaller. As shown in Fig. 5, our theoretical calculation results are consistent with the intuitive analysis. Similarly, for T_2 molecules, the asymmetry parameter is even smaller.

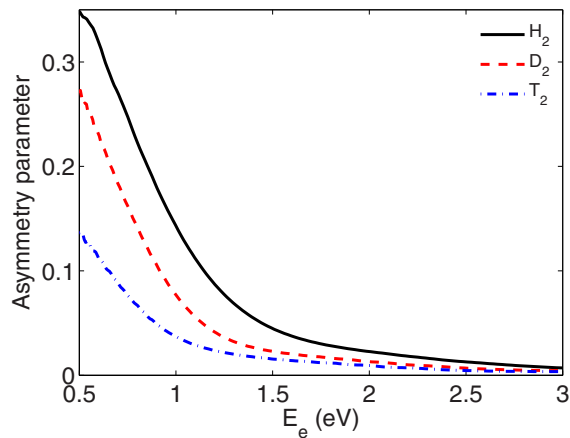


FIG. 5. The asymmetry parameter δ as a function of the ejected electron energy E_e for isotope molecules H_2 , D_2 , and T_2 in the same laser field with photon energy 21.1 eV.

IV. CONCLUSION

In conclusion, we studied the asymmetric electron localization in the dissociative ionization of H_2 in an XUV field. After the single-photon single ionization of H_2 , the freed electron and the dissociative H_2^+ may have the Coulomb interaction, leading to the transition between $1s\sigma_g$ and $2p\sigma_u$ states in H_2^+ . The mixture of these two states with opposite parities determines the asymmetric electron localization on the two nuclei after dissociation of H_2^+ . The asymmetry parameter

depends on the free electron energy, and thus the nuclear energy since the nuclei and the freed electron have shared the photo energy. Generally, if the free electron moves slower, the Coulomb interaction between the free electron and H_2^+ is stronger, and the asymmetry parameter is larger. The bound electron in H_2^+ prefers being located on the nucleus moving in the opposite the direction of the freed electron. This result is consistent with the intuitive picture that two electrons repel each other wherever they are. Though the numerical model restricts all dynamics along the molecular axis, and thus cannot accurately describe electron-electron correlation, ionization probability, and so on, the simulation results obtained by such a reduced-dimensionality model agree with the experimental measurement in all energy ranges. We believe that the one-dimensional model can grasp the main physics and thus can be used to explore more physics about H_2 and its isotopic molecules.

ACKNOWLEDGMENTS

This work was supported by the Innovation Program of Shanghai Municipal Education Commission (Grant No. 2017-01-07-00-02-E00034), National Key R&D Program of China (Grant No. 2018YFA0404802), National Natural Science Foundation of China (NSFC) (Grants No. 11925405, No. 11721091, and No. 91850203), and the Natural Science Foundation of Liaoning Province (Grant No. 2020-BS-078). Simulations were performed on the π supercomputer at Shanghai Jiao Tong University.

-
- [1] A. Palacios, J. L. Sanz-Vicario, and F. Martín, *J. Phys. B* **48**, 242001 (2015).
- [2] H. Ibrahim, C. Lefebvre, A. D. Bandrauk, A. Staudte, and F. Légaré, *J. Phys. B* **51**, 042002 (2018).
- [3] W. Zhang, P. Lu, J. Ma, H. Li, X. Gong, and J. Wu, *J. Phys. B* **53**, 162001 (2020).
- [4] R. Y. Bello, S. E. Canton, D. Jelovina, J. D. Bozek, B. Rude, O. Smirnova, M. Y. Ivanov, A. Palacios, and F. Martín, *Sci. Adv.* **4**, eaat3962 (2018).
- [5] L. Cattaneo, J. Vos, R. Y. Bello, A. Palacios, S. Heuser, L. Pedrelli, M. Lucchini, C. Cirelli, F. Martín, and U. Keller, *Nat. Phys.* **14**, 733 (2018).
- [6] W. Zhang, X. Gong, H. Li, P. Lu, F. Sun, Q. Ji, K. Lin, J. Ma, H. Li, J. Qiang, F. He, and J. Wu, *Nat. Commu.* **10**, 757 (2019).
- [7] O. I. Tolstikhin, H. J. Wörner, and T. Morishita, *Phys. Rev. A* **87**, 041401(R) (2013).
- [8] X. Wang, H. Xu, A. Atia-Tul-Noor, B. T. Hu, D. Kielpinski, R. T. Sang, and I. V. Litvinyuk, *Phys. Rev. Lett.* **117**, 083003 (2016).
- [9] M. Lein, *Phys. Rev. Lett.* **94**, 053004 (2005).
- [10] S. Baker, J. S. Robinson, C. A. Haworth, H. Teng, R. A. Smith, C. C. Chirilă, M. Lein, J. W. G. Tisch, and J. P. Marangos, *Science* **312**, 424 (2006).
- [11] P. F. Lan, M. Ruhmann, L. X. He, C. Y. Zhai, F. Wang, X. S. Zhu, Q. B. Zhang, Y. M. Zhou, M. Li, M. Lein, and P. X. Lu, *Phys. Rev. Lett.* **119**, 033201 (2017).
- [12] M. F. Kling, Ch. Siedschlag, A. J. Verhoef, J. I. Khan, M. Schultze, Th. Uphues, Y. Ni, M. Uiberacker, M. Drescher, F. Krausz, and M. J. J. Vrakking, *Science* **312**, 246 (2006).
- [13] V. Roudnev, B. D. Esry, and I. Ben-Itzhak, *Phys. Rev. Lett.* **93**, 163601 (2004).
- [14] D. Ray, F. He, S. De, W. Cao, H. Mashiko, P. Ranitovic, K. P. Singh, I. Znakovskaya, U. Thumm, G. G. Paulus, M. F. Kling, I. V. Litvinyuk, and C. L. Cocke, *Phys. Rev. Lett.* **103**, 223201 (2009).
- [15] F. He, C. Ruiz, and A. Becker, *Phys. Rev. Lett.* **99**, 083002 (2007).
- [16] G. Sansone, F. Kelkensberg, J. F. Pérez-Torres, F. Morales, M. F. Kling, W. Siu, O. Ghafur, P. Johnsson, M. Swoboda, E. Benedetti, F. Ferrari, F. Lépine, J. L. Sanz-Vicario, S. Zherebtsov, I. Znakovskaya, A. L'Huillier, M. Yu. Ivanov, M. Nisoli, F. Martín, and M. J. J. Vrakking, *Nature (London)* **465**, 763 (2010).
- [17] F. He, C. Ruiz, and A. Becker, *J. Phys. B* **41**, 081003 (2008).
- [18] K. P. Singh, F. He, P. Ranitovic, W. Cao, S. De, D. Ray, S. Chen, U. Thumm, A. Becker, M. M. Murnane, H. C. Kapteyn, I. V. Litvinyuk, and C. L. Cocke, *Phys. Rev. Lett.* **104**, 023001 (2010).
- [19] J. Wu, M. Magrakvelidze, L. P. H. Schmidt, M. Kunitski, T. Pfeifer, M. Schöffler, M. Pitzer, M. Richter, S. Voss, H. Sann,

- H. Kim, J. Lower, T. Jahnke, A. Czasch, U. Thumm, and R. Dörner, *Nat. Commun.* **4**, 2177 (2013).
- [20] J. Wu, A. Vredenburg, L. Ph. H. Schmidt, T. Jahnke, A. Czasch, and R. Dörner, *Phys. Rev. A* **87**, 023406 (2013).
- [21] X. Gong, P. He, Q. Song, Q. Ji, H. Pan, J. Ding, F. He, H. Zeng, and J. Wu, *Phys. Rev. Lett.* **113**, 203001 (2014).
- [22] B. Fischer, M. Kremer, T. Pfeifer, B. Feuerstein, V. Sharma, U. Thumm, C. D. Schröter, R. Moshhammer, and J. Ullrich, *Phys. Rev. Lett.* **105**, 223001 (2010).
- [23] M. Kremer, B. Fischer, B. Feuerstein, V. L. B. de Jesus, V. Sharma, C. Hofrichter, A. Rudenko, U. Thumm, C. D. Schröter, R. Moshhammer, and J. Ullrich, *Phys. Rev. Lett.* **103**, 213003 (2009).
- [24] F. Anis and B. D. Esry, *Phys. Rev. Lett.* **109**, 133001 (2012).
- [25] V. V. Serov and A. S. Kheifets, *Phys. Rev. A* **89**, 031402(R) (2014).
- [26] M. Waitz, D. Aslittürk, N. Wechselberger, H. K. Gill, J. Rist, F. Wiegandt, C. Goihl, G. Kastirke, M. Weller, T. Bauer, D. Metz, F. P. Sturm, J. Voigtsberger, S. Zeller, F. Trinter, G. Schiwietz, T. Weber, J. B. Williams, M. S. Schöffler, L. Ph. H. Schmidt, T. Jahnke, and R. Dörner, *Phys. Rev. Lett.* **116**, 043001 (2016).
- [27] S. Heck, A. Gatton, K. A. Larsen, W. Iskandar, E. G. Champenois, R. Strom, A. Landers, D. Reedy, C. Dailey, J. B. Williams, T. Severt, B. Jochim, I. Ben-Itzhak, R. Moshhammer, R. Dörner, D. S. Slaughter, and Th. Weber, *Phys. Rev. Res.* **1**, 033140 (2019).
- [28] J. P. Wang and F. He, *Phys. Rev. A* **97**, 043411 (2018).
- [29] Z. C. Li and F. He, *Phys. Rev. A* **90**, 053423 (2014).
- [30] P. Lu, J. Wang, H. Li, K. Lin, X. Gong, Q. Song, Q. Ji, W. Zhang, J. Ma, H. X. Li, H. Zeng, F. He, and J. Wu, *Proc. Natl. Acad. Sci. USA* **115**, 2049 (2018).
- [31] S. Saugout, C. Cornaggia, A. Suzor-Weiner, and E. Charron, *Phys. Rev. Lett.* **98**, 253003 (2007).
- [32] S. Saugout, E. Charron, and C. Cornaggia, *Phys. Rev. A* **77**, 023404 (2008).
- [33] A. D. Bandrauk, S. Chelkowski, and H. Lu, *J. Phys. B* **42**, 075602 (2009).
- [34] M. N. Daud, H. Lu, S. Chelkowski, and A. D. Bandrauk, *Int. J. Quantum Chem.* **115**, 369 (2015).
- [35] R. Kosloff and D. Kosloff, *J. Comput. Phys.* **63**, 363 (1986).
- [36] W. H. Press, S. A. Teukolsky, W. T. Vetterling, and B. P. Flannery, *Numerical Recipes* (Cambridge University Press, Cambridge, England, 1992).
- [37] K. J. Schafer and K. C. Kulander, *Phys. Rev. A* **42**, 5794 (1990).
- [38] A. Lafosse, M. Lebech, J. C. Brenot, P. M. Guyon, L. Spielberger, O. Jagutzki, J. C. Houver, and D. Dowek, *J. Phys. B* **36**, 4683 (2003).
- [39] D. Dowek, J. F. Pérez-Torres, Y. J. Picard, P. Billaud, C. Elkharrat, J. C. Houver, J. L. Sanz-Vicario, and F. Martín, *Phys. Rev. Lett.* **104**, 233003 (2010).
- [40] J. F. Pérez-Torres, J. L. Sanz-Vicario, K. Veyrinas, P. Billaud, Y. J. Picard, C. Elkharrat, S. M. Poullain, N. Saquet, M. Lebech, J. C. Houver, F. Martin, and D. Dowek, *Phys. Rev. A* **90**, 043417 (2014).
- [41] S. K. Semenov and N. A. Cherepkov, *J. Phys. B* **36**, 1409 (2003).
- [42] J. Fernández and F. Martín, *New J. Phys.* **11**, 043020 (2009).